Prepared for submission to JHEP

KCL-PH-TH/2014-39
LCTS/2014-38

Prospects for observing charginos and neutralinos at a 100 TeV proton-proton collider

Bobby S. Acharya,[a,b] **Krzysztof Bożek,**[a] **Chakrit Pongkitivanichkul,**[a] **Kazuki Sakurai**[a]

[a] *Theoretical Particle Physics & Cosmology, Department of Physics, King's College London, London, WC2R 2LS, United Kingdom*

[b] *The Abdus Salam International Centre for Theoretical Physics, Trieste, Italy*

E-mail: bobby.acharya@kcl.ac.uk, krzysztof.bozek@kcl.ac.uk, chakrit.pongkitivanichkul@kcl.ac.uk, kazuki.sakurai@kcl.ac.uk

Abstract: We investigate the prospects for discovering charginos and neutralinos at a future pp collider with $\sqrt{s} = 100$ TeV. We focus on models where squarks and sleptons are decoupled – as motivated by the LHC data. Our initial study is based on models where Higgsinos form the main component of the LSP and W-inos compose the heavier chargino states ($M_2 > \mu$), though it is straightforward to consider the reverse situation also. We show that in such scenarios W-inos decay into $W^{\pm}$, Z and h plus neutralinos almost universally. In the WZ channel we compare signal and background in various kinematical distributions. We design simple but effective signal regions for the trilepton channel and evaluate discovery reach and exclusion limits. Assuming 3000 fb^{-1} of integrated luminosity, W-inos could be discovered (excluded) up to 1.1 (1.8) TeV if the spectrum is not compressed.

Keywords: Supersymmetry, Hadron-Hadron Scattering

arXiv:1410.1532v1 [hep-ph] 6 Oct 2014

Contents

1 Introduction **1**

2 The cross sections and branching ratios **2**
2.1 The model setup 2
2.2 The cross sections 3
2.3 The branching ratios 4

3 The simulation setup **5**

4 The kinematic distributions **8**

5 The limit and discovery reach **9**
5.1 The event selection 9
5.2 The result 10

6 Conclusion **12**

A The lepton isolation requirement **13**

B The visible cross sections **14**

1 Introduction

Supersymmetry is one of the most promising ideas for physics beyond the Standard Model, since it directly addresses the hierarchy problem. In its minimal incarnation, the MSSM, the chargino-neutralino sector is particularly important for several phenomenological reasons. Firstly, this sector contains Higgsinos, whose mass parameter, μ, plays a crucial role in electroweak symmetry breaking. If the MSSM provides a solution to the gauge hierarchy problem, at least some of the charginos and neutralinos must be present not too far from the electroweak scale. Secondly, many SUSY breaking scenarios suggest that one of the neutralinos becomes the lightest SUSY particle (LSP). Typically, the lightest neutralino is stable due to a discrete symmetry (e.g. R-parity) and might be a promising candidate for dark matter. Such a stable neutralino also plays a crucial role in the collider phenomenology since the decay of supersymmetric particles will always produce the LSP, leading to a distinctive missing energy signature.

The ATLAS and CMS experiments at the CERN Large Hadron Collider (LHC) have put considerable effort into looking for charginos and neutralinos in the LHC data. In hadron colliders the expected limit and discovery reach for the charginos and neutralinos are considerably weaker compared to those for squarks and gluinos. For the $\tilde{\chi}_1^{\pm}\tilde{\chi}_2^0 \to W^{\pm}\tilde{\chi}_1^0 Z\tilde{\chi}_1^0$

simplified model with $m_{\tilde{\chi}_1^\pm} = m_{\tilde{\chi}_2^0}$ and $m_{\tilde{\chi}_1^0} = 0$ GeV, the current limit is $m_{\tilde{\chi}_1^\pm} \gtrsim 400$ GeV [1, 2]. The projection for the 14 TeV LHC has been estimated for the same simplified model by ATLAS [3]. The 5-σ discovery reach (95% CL limit) for the chargino mass is about 550 (880) GeV for 300 fb^{-1} and 800 (1100) GeV for 3000 fb^{-1}. For massive neutralinos ($m_{\tilde{\chi}_1^0} > 0$ GeV) or models with BR($\tilde{\chi}_2^0 \to h\tilde{\chi}_1^0$) > 0, the limit and discovery reach become even weaker. These limits are well below those required by typical dark matter model.

Recently, there has been discussion of the next generation of circular colliders, including high energy proton-proton machines. Several physics cases at proton-proton colliders with $\sqrt{s} \simeq 100$ TeV have already been studied [4–12]. In particular, the limit and discovery reach for coloured SUSY particles have been studied in the context of simplified models assuming a 100 TeV proton-proton collider with 3000 fb^{-1} of integrated luminosity [4]. The mono-jet search [9] as well as the mono-photon, soft lepton and disappearing track searches [11, 12] have been studied in the similar setup for production of the pure W-inos (Higgsinos), assuming they are the main component of the LSP. The 100 TeV colliders will provide a great opportunity to discover heavier charginos and neutralinos beyond the LHC reach.

In this paper we study chargino-neutralino search at a 100 TeV collider assuming 3000 (1000) fb^{-1} luminosity exploiting the WZ channel. In stead of employing a simplified model approach, we work on a model which may arise as a limit of concrete models. In particular we assume $M_2 > \mu > 0$ and $M_2 - \mu \gg m_Z$, where M_2 is the W-ino mass and μ is the Higgsino mass. In this scenario Higgsinos form the main component of the lighter charginos and neutralinos ($\tilde{\chi}_1^\pm, \tilde{\chi}_1^0, \tilde{\chi}_2^0 \sim \widetilde{H}^\pm, \widetilde{H}_1^0, \widetilde{H}_2^0$) and W-inos compose the heavier charginos and neutralinos ($\tilde{\chi}_1^\pm, \tilde{\chi}_3^0 \sim \widetilde{W}^\pm, \widetilde{W}^0$). This assumption is partly motivated by naturalness, by anomaly mediation SUSY breaking scenarios, by string/M theory models and by split supersymmetry [13–21]

The rest of the paper is organised as follows. In section 2, we describe the model setup and study the production cross sections and branching ratios of charginos and neutralinos. After clarifying our simulation setup in section 3, various kinematic distributions for signal and background are studied in section 4, which will be used to design optimal event selection cuts for the chargino-neutralino search. In section 5, we present the result of our analysis and derive the limit and discovery reach in the $M_2 - \mu$ parameter plane. The conclusions are given in section 6.

2 The cross sections and branching ratios

2.1 The model setup

In this paper we focus on the models with $M_2 > \mu > 0$ and $M_2 - \mu \gg m_Z$, where the μ is the mass of the Higgsinos and M_2 is the mass of the W-inos since the W-ino production cross-section is larger than the Higgsino cross-section. We assume that all the other SUSY particles, including the B-ino, are decoupled and all SUSY breaking parameters are real for simplicity. In this situation the mixing between W-ino and Higgsino is negligible; the two Higgsino doublets are the lightest charginos and the two lightest neutralinos (which

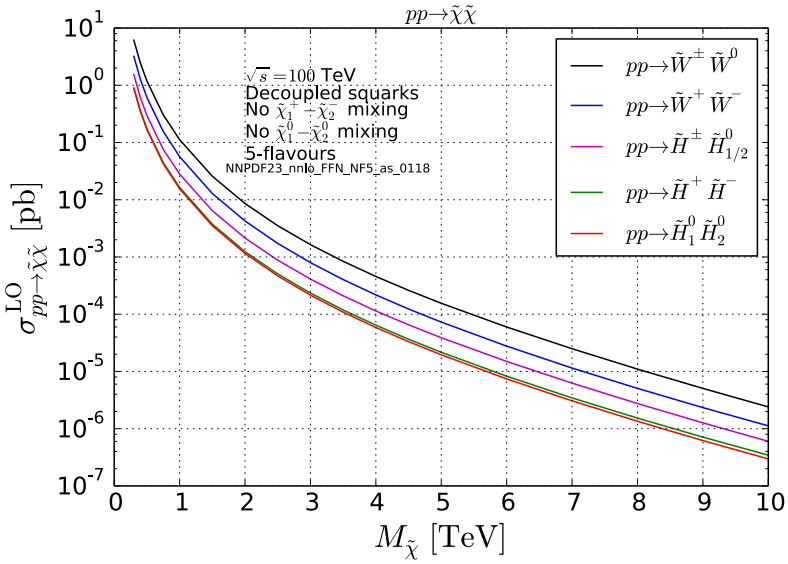

Figure 1. The leading order cross sections for the W-ino and Higgsino pair productions at a 100 TeV proton-proton collider with decoupled squarks and sleptons.

are almost degenerate) and the W-inos (SU(2) triplet) are the second lightest charginos and the third lightest neutralino (almost mass degenerate):

$$\begin{aligned} \tilde{\chi}_1^\pm, \tilde{\chi}_1^0, \tilde{\chi}_2^0 &\sim \widetilde{H}^\pm, \widetilde{H}_1^0, \widetilde{H}_2^0 \quad \text{with} \quad m_{\tilde{\chi}_1^\pm} \simeq m_{\tilde{\chi}_1^0} \simeq m_{\tilde{\chi}_2^0} \simeq |\mu|, \\ \tilde{\chi}_2^\pm, \tilde{\chi}_3^0 &\sim \widetilde{W}^\pm, \widetilde{W}^0 \quad \text{with} \quad m_{\tilde{\chi}_2^\pm} \simeq m_{\tilde{\chi}_3^0} \simeq |M_2|, \end{aligned} \tag{2.1}$$

where $\widetilde{H}_{1/2}^0 = \frac{1}{\sqrt{2}}(\widetilde{H}_u^0 \mp \widetilde{H}_d^0)$ is the neutral Higgsino mass eigenstate. With this setup, the remaining free parameters are M_2, μ and $\tan\beta$. We use $\tan\beta = 10$ throughout our numerical study. However, the impact of $\tan\beta$ on the production cross section and branching ratio of the charginos and neutralinos that are W-ino or Higgsino like is almost negligible unless $\tan\beta$ is extremely small. We therefore believe our results including the chargino-neutrino mass reach are still useful for other values of $\tan\beta$.

2.2 The cross sections

We show the leading order (LO) cross sections for the W-ino and Higgsino pair productions at a 100 TeV proton-proton collider in Fig. 1. The cross sections are calculated using `MadGraph 5` [22]. Since squarks are decoupled, the W-inos and Higgsinos are produced via the s-channel diagrams exchanging off-shell $W^\pm$ and Z bosons. For the pure W-inos and Higgsinos, there is no associated W-ino-Higgsino production process. Pair production of the same neutralino states, $\widetilde{W}^0\widetilde{W}^0$, $\widetilde{H}_1^0\widetilde{H}_1^0$, $\widetilde{H}_2^0\widetilde{H}_2^0$, are also absent.

One can see that the $\widetilde{W}^\pm\widetilde{W}^0$ production mode has the largest cross section. The LO cross section varies from 10^3 fb to 10^{-2} fb for the W-ino mass from 500 GeV to 8 TeV.

2.3 The branching ratios

The W-ino-Higgsino interaction is derived from the kinetic terms of Higgsinos.

$$\begin{aligned}\mathcal{L} &\supset \left[H_u^\dagger e^V H_u + H_d^\dagger e^V H_d\right]_{\theta^4} \\ &\supset \sqrt{2}g(H_u^* \widetilde{W}^a T^a \widetilde{H}_u - H_d^* \widetilde{W}^a T^a \widetilde{H}_d) + \text{h.c.}\ . \end{aligned} \tag{2.2}$$

The Higgs and Higgsino fields can be written in terms of the Goldstone bosons and the mass eigenstates as:

$$\begin{aligned}\begin{pmatrix} H_u^+ \\ H_u^0 \end{pmatrix} &= \begin{pmatrix} \sin\beta \cdot \phi^+ + \cdots \\ \frac{1}{\sqrt{2}}(\cos\alpha \cdot h + i \sin\beta \cdot \phi^0) + \cdots \end{pmatrix}, \quad \begin{pmatrix} \widetilde{H}_u^+ \\ \widetilde{H}_u^0 \end{pmatrix} \simeq \begin{pmatrix} \widetilde{H}^+ \\ \frac{1}{\sqrt{2}}(\widetilde{H}_1^0 + i\widetilde{H}_2^0) \end{pmatrix}, \\ \begin{pmatrix} H_d^0 \\ H_d^- \end{pmatrix} &= \begin{pmatrix} \frac{-1}{\sqrt{2}}(\sin\alpha \cdot h + i\cos\beta \cdot \phi^0) + \cdots \\ -\cos\beta \cdot \phi^- + \cdots \end{pmatrix}, \quad \begin{pmatrix} \widetilde{H}_d^0 \\ \widetilde{H}_d^- \end{pmatrix} \simeq \begin{pmatrix} \frac{1}{\sqrt{2}}(\widetilde{H}_1^0 - i\widetilde{H}_2^0) \\ \widetilde{H}^- \end{pmatrix}, \end{aligned} \tag{2.3}$$

where h is the SM like Higgs boson, and ϕ^0 and $\phi^\pm$ are the Goldstone bosons to be eaten by the SM gauge bosons, Z and $W^\pm$, respectively. The angles α and β represent the mixing for the neutral and charged Higgs mass matrices.

In the large $\tan\beta$ limit, we have $\cos\alpha/\sin\alpha \simeq (-\sin\beta)/\cos\beta$, and one can see that the $h\widetilde{W}\widetilde{H}$, $\phi^0\widetilde{W}\widetilde{H}$ and $\phi^\pm\widetilde{W}\widetilde{H}$ have the same coupling. In this limit one can find the following results using the Goldstone equivalence theorem [23].

$$\begin{aligned}\text{BR}(\widetilde{W}^\pm) &\simeq \begin{cases} 0.5 & \to W^\pm \widetilde{H}_1^0 \text{ or } W^\pm \widetilde{H}_2^0 \\ 0.25 & \to h\widetilde{H}^\pm \\ 0.25 & \to Z\widetilde{H}^\pm \end{cases} \\ \text{BR}(\widetilde{W}^0) &\simeq \begin{cases} 0.5 & \to W^\pm \widetilde{H}^\mp \\ 0.25 & \to h\widetilde{H}_1^0 \text{ or } h\widetilde{H}_2^0 \\ 0.25 & \to Z\widetilde{H}_1^0 \text{ or } Z\widetilde{H}_2^0 \end{cases}. \end{aligned} \tag{2.4}$$

The different CP properties between h and ϕ^0, and $\widetilde{H}_1^0$ and $\widetilde{H}_2^0$ result in the different rates for $\widetilde{W}^0 \to h\widetilde{H}_1^0$ and $\widetilde{W}^0 \to Z\widetilde{H}_1^0, h\widetilde{H}_2^0$. These rates are given by

$$\begin{aligned}\text{BR}(\widetilde{W}^\pm \to W^\pm \widetilde{H}_1^0) &\simeq \text{BR}(\widetilde{W}^\pm \to W^\pm \widetilde{H}_2^0), \\ \text{BR}(\widetilde{W}^0 \to h\widetilde{H}_{1/2}^0) &\simeq \text{BR}(\widetilde{W}^0 \to Z\widetilde{H}_{2/1}^0), \\ \frac{\text{BR}(\widetilde{W}^0 \to Z\widetilde{H}_1^0)}{\text{BR}(\widetilde{W}^0 \to h\widetilde{H}_1^0)} &\simeq \frac{1-2|\mu/M_2|}{1+2|\mu/M_2|}\ . \end{aligned} \tag{2.5}$$

Fig. 2 shows the branching ratios of $\widetilde{W}^\pm$ and $\widetilde{W}^0$, which have been calculated using `SUSY-HIT` [24]. One can see that the branching ratios approach Eq. (2.4) in the large M_2 limit. For the region where $|M_2 - \mu|$ is close to the masses of SM bosons, the decay mode into $W^\pm$ enhances since it has the largest phase space factor.

Since the charged and neutral W-inos are almost mass degenerate, it may not be possible to resolve $\widetilde{W}^\pm \to XY$ and $\widetilde{W}^0 \to X'Y'$ in hadron colliders if XY is equal to $X'Y'$

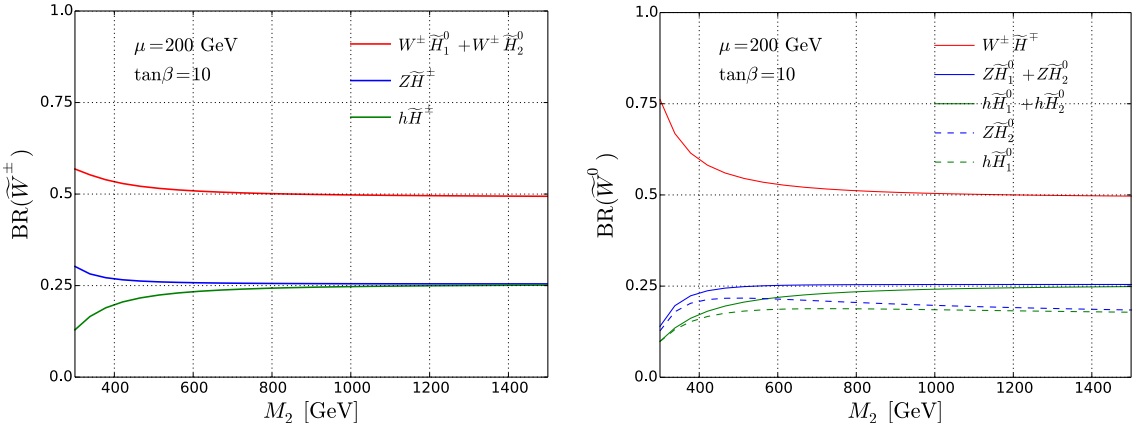

(a) (b)

Figure 2. The branching ratios of $\widetilde{W}^\pm$ **(a)** and $\widetilde{W}^0$ **(b)** as functions of M_2. The μ parameter is fixed at 200 GeV. The SUSY particles other than W-inos and Higgsinos are decoupled.

up to soft activities. Similarly, four degenerate Higgsinos would not be resolvable, since $\widetilde{H}^\pm$ and $\widetilde{H}_2^0$ usually decay promptly into $\widetilde{H}_1^0$ and their decay products are too soft to be detected. We therefore categorise the processes into distinguishable groups in terms of the SM bosons appearing in the final states. For example, $\chi'\chi' \to WZ\chi\chi$ process (WZ mode) includes $\widetilde{W}^+\widetilde{W}^- \to (W^\pm\widetilde{H}_{1/2}^0)(Z\widetilde{H}^\mp)$, $\widetilde{W}^\pm\widetilde{W}^0 \to (W^\pm\widetilde{H}_{1/2}^0)(Z\widetilde{H}_{1/2}^0)$, $(Z\widetilde{H}^\pm)(W^\pm\widetilde{H}^\mp)$ and $\widetilde{W}^0\widetilde{W}^0 \to (W^\pm\widetilde{H}^\mp)(Z\widetilde{H}_{1/2}^0)$. We show the cross sections of the all 6 distinguishable modes, WZ, Wh, WW, ZZ, Zh and hh modes, in the $M_2 - \mu$ plane in Fig. 3.

One can see that the modes containing at least one W have considerably larger cross sections compared to the others at the same mass point. In particular, the WZ mode is promising[1] because one can reduce the QCD and $t\bar{t}$ backgrounds significantly by requiring three high p_T leptons (See Fig. 4.). Taking advantage of this we henceforth study the expected discovery reach and exclusion limit for chargino-neutralino production in the WZ mode.

In Fig. 5, we show the cross section of the WZ mode after taking account of the branching ratios of the gauge bosons into $3\ell + \nu$. The black curve represents the limit beyond which less than 5 signal events ($\chi'\chi' \to WZ\chi\chi \to 3\ell\nu\chi\chi$) are produced, assuming the integrated luminosity of 3000 fb^{-1}. This provides a rough estimate of the theoretically maximum possible exclusion limit assuming zero background with perfect signal efficiency.

3 The simulation setup

We use the Snowmass background samples [30] to estimate the Standard Model (SM) backgrounds. We include the relevant SM processes, which are summarised in Table 1.

[1] The Wh mode is also interesting. See [25–29] for some recent studies.

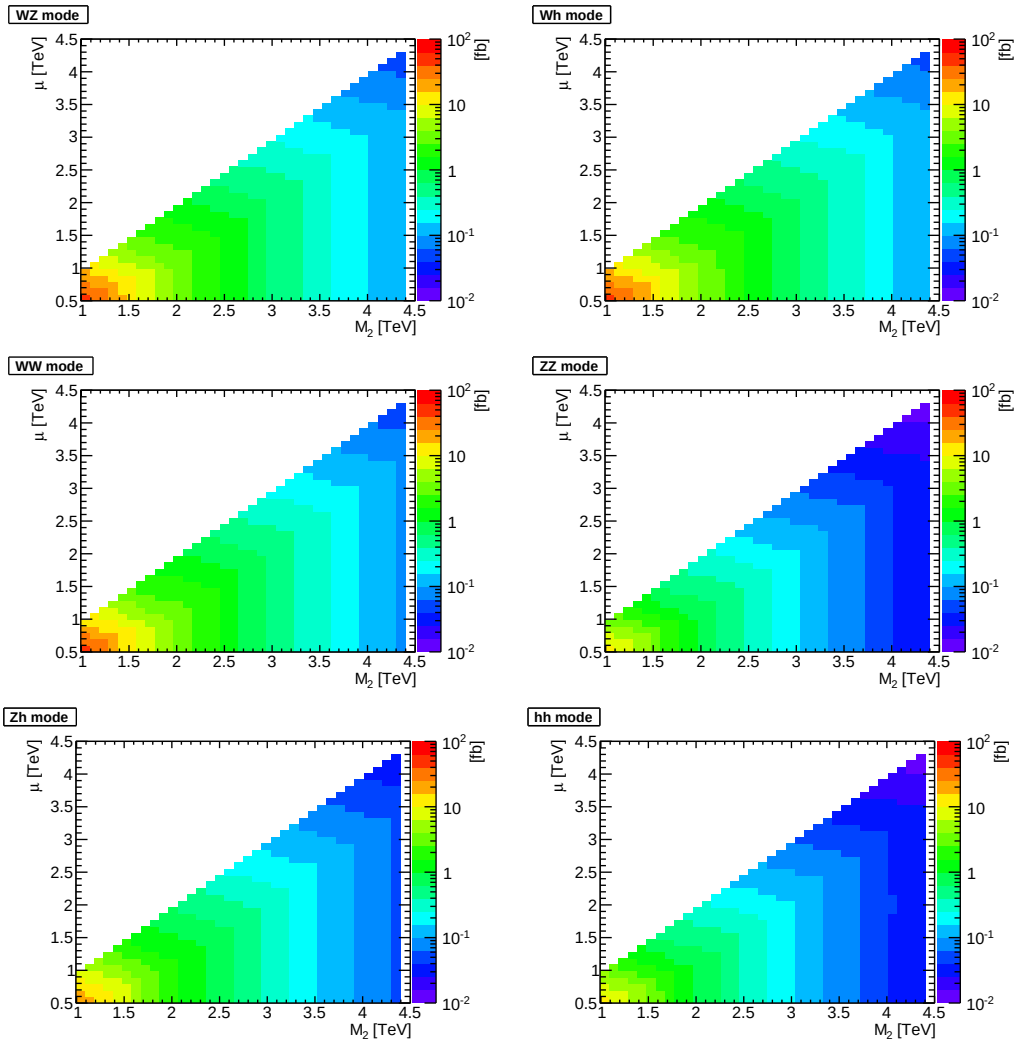

Figure 3. The cross sections of the 6 distinguishable modes, $\chi'\chi' \to XY\chi\chi$ with $XY = WZ, Wh, WW, ZZ, Zh$ and hh, as functions of M_2 and μ. SUSY particles other than W-inos and Higgsinos are decoupled.

For signal events we first generate chargino and neutralino production events using `MadGraph 5` with the parameters obtained by `SUSY-HIT`. We consider two production processes $pp \to \chi_2^+\chi_2^-$ and $pp \to \chi_2^\pm\chi_3^0$, where $\chi_2^\pm \sim \widetilde{W}^\pm$ and $\chi_3^0 \sim \widetilde{W}^0$. The generated samples are then passed to `BRIDGE` [31] to have the charginos and neutralinos decay. We then only accept the events with W and Z in the final states, and pass those events once again to `BRIDGE` to let W and Z decay leptonicaly. Finally we simulate the effects of parton shower, hadronization and detector resolutions using `Pythia 6` [32] and `Delphes 3` [33]. The detector simulation is tuned according to the Snowmass detector framework [30].

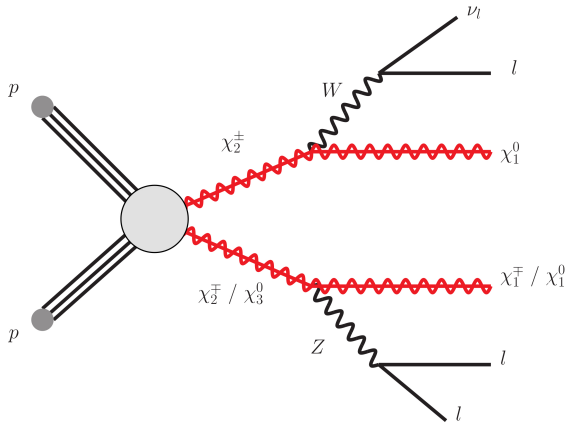

Figure 4. The dominant event topology for signal events.

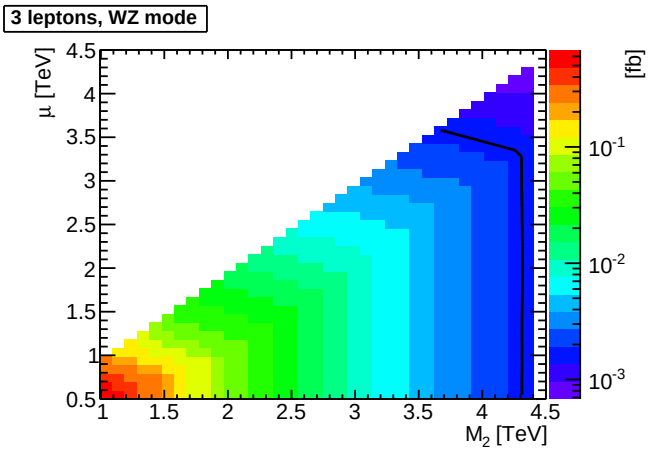

Figure 5. The cross section of $\chi'\chi' \to WZ\chi\chi \to 3\,\ell\nu\chi\chi$ as a function of M_2 and μ. The black curve represents the limit beyond which less than 5 signal events are produced, assuming the integrated luminosity of 3000 fb^{-1}.

Name	Snowmass	Relavant sub-processes	$\sigma_{\text{total}}^{\text{NLO}}$ [pb]
diboson	VV	W^+W^-, $W^{\pm}Z$, ZZ	430.5
top-pair + gauge boson	ttV	$t\bar{t}W^{\pm}$, $t\bar{t}Z$, $t\bar{t}\,h$	219.9
top + gauge boson	tV	$tW^{\pm}$, $\bar{t}W^{\pm}$	182.5
triple gauge boson	VVV	$W^+W^-W^{\pm}$, W^+W^-Z, $W^{\pm}ZZ$, ZZZ	36.4

Table 1. The Standard Model background included in the analysis. For each background category, we only list sub-processes relevant in the 3 lepton analysis. Reported cross sections include all sub-processes in corresponding background categories.

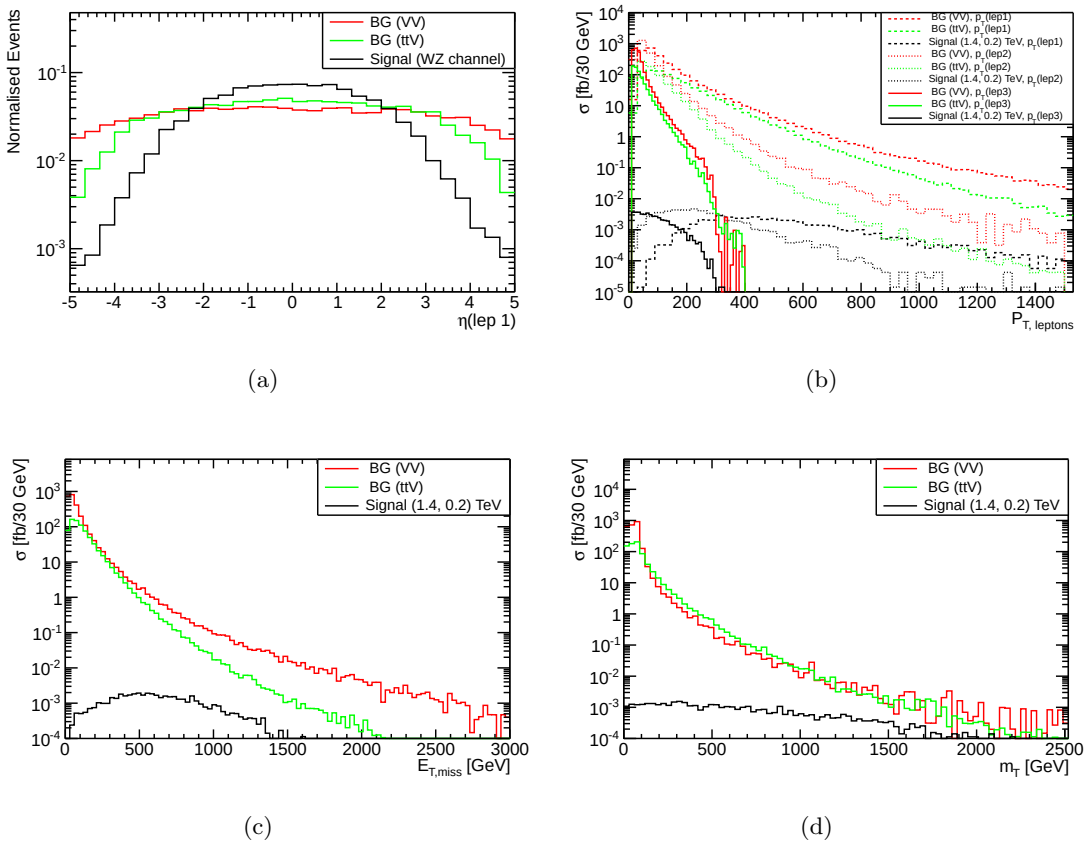

Figure 6. The distributions of **(a)** the leading lepton pseudo-rapidity, η_{ℓ_1}, **(b)** p_T of the three hardest leptons, **(c)** the missing transverse energy, $E_T^{\rm miss}$, **(d)** the transverse mass, m_T. The backgrounds are diboson (VV) and associated top-pair plus vector boson production (ttV). The signal events are generated at our benchmark point, $M_2 = 1.4$ TeV and $\mu = 200$ GeV, and only WZ mode is considered. The parton level events are used for **(a)**, whilst the detector level events after applying the 3 lepton + SFOS cuts are used for **(b)**, **(c)** and **(d)**.

4 The kinematic distributions

In this section we show some kinematic distributions for the background and signal events. We consider the WZ mode for signal and diboson (VV) and top-pair plus gauge boson (ttV) processes for backgrounds. The signal distributions are generated at a benchmark point: $M_2 = 1.4$ TeV, $\mu = 200$ GeV. Throughout this section we use a notation denoting the i-th hardest lepton (electron or muon) by ℓ_i (namely, $p_T(\ell_i) > p_T(\ell_j)$ for $i < j$).

Fig. 6(a) shows the normalised distributions of the leading lepton pseudo-rapidity, η_{ℓ_1}, for signal (black) and background (red for VV and green for ttV). The distributions are obtained at a parton level without selection cuts apart from $p_T(\ell_1) > 10$ GeV to understand the bare distribution before taking the detector acceptance into account. One can see that the leptons in the background tend to be more forward compared to the signal leptons. The production threshold is much lower for the backgrounds and more asymmetric

momentum configurations are allowed for the initial partons. If one of the initial partons has a much larger momentum than the other, the system is boosted in the direction of the beam pipe and the leptons tend to be produced in the forward region.[2] Another effect is as follows. Unlike the signal, production of the backgrounds have a contribution from t-channel diagrams. In 100 TeV colliders, the SM gauge bosons can effectively be regarded as "massless" particles and there is an enhancement in the region of the phase space where the gauge bosons are produced in the forward region.

Fig. 6(b) shows the p_T distributions of the three hardest leptons. The distributions are obtained after taking the hadronization and detector effects into account and requiring at least 3 leptons (with $p_T > 10$ GeV, $|\eta| < 2.5$), of which two are same flavour and opposite sign (SFOS). As can be seen, the p_T-spectrum of background leptons has peaks below 100 GeV, whilst the signal peaks at around 300, 150 and $\lesssim 50$ GeV for the leading, second leading and third leading leptons for our benchmark point.

We also show the $E_T^{\rm miss}$ distributions in Fig. 6(c), where we use the same event sample as those in Fig. 6(b). The main source of the $E_T^{\rm miss}$ in the background are the neutrinos produced from W and Z decays and the distribution has a peak around $30-40$ GeV. Above this peak, the background $E_T^{\rm miss}$ distribution falls quickly. On the other hand, a large $E_T^{\rm miss}$ can be produced from the signal from the decays of heavy charginos and neutralinos. The typical scale of $E_T^{\rm miss}$ is given by $\sim M_2/2$. As can be seen, the signal distribution has a peak around 500 GeV. This indicates that a hard cut on $E_T^{\rm miss}$ will greatly help to improve the signal to background ratio.

We show the transverse mass m_T distributions in Fig. 6(d), where the event samples are again the same as those used in Fig. 6(b). We define $m_T \equiv \sqrt{2|p_T(\ell')||E_T^{\rm miss}|(1-\cos\Delta\phi)}$, where ℓ' is the hardest lepton amongst those not chosen as the SFOS lepton pair and $\Delta\phi$ is the azimuthal difference between the ℓ' and the direction of $\overrightarrow{p}_T^{\rm miss}$. In the WZ background, this distribution has an endpoint at m_W and above the endpoint the distribution drops very sharply. In the signal events, the distributions are much broader, as can be seen in Fig. 6(d). A harsh cut on m_T would also be very helpful to reject a large fraction of background without sacrificing too many signal events.

5 The limit and discovery reach

5.1 The event selection

Our event selection consists of two parts: *preselection* and *signal region* (*SR*) *selection*. The *preselection* requirement is:

- exactly three isolated leptons with $p_T > 10$ GeV and $|\eta| < 2.5$
- a same-flavour opposite-sign (SFOS) lepton pair with $|m_{\ell\ell}^{\rm SFOS} - m_Z| < 10$ GeV
- no b-tagged jet

[2] For the W^+Z background, the initial state is often u and $\bar{d}$. If the partonic collision energy is much smaller than the proton-proton collision energy, it is more likely to find a valence quark u carrying a larger fraction of the proton momentum compared to the sea quark $\bar{d}$.

Signal Region	3 lepton p_T [GeV]	$E_T^{\rm miss}$ [GeV]	m_T [GeV]
Loose	$> 100, 50, 10$	> 150	> 150
Medium	$> 250, 150, 50$	> 350	> 300
Tight	$> 400, 200, 75$	> 800	> 1100

Table 2. The event selection cuts required in the signal regions. These cuts are applied on top of the preselection cuts.

With the first condition one can effectively reject the QCD, hadronic $t\bar{t}$ and single gauge boson backgrounds. The definition of lepton isolation and some discussion around it is given in Appendix A. The second condition is introduced to remove the leptonic SM processes without Z bosons, such as $t\bar{t}W^{\pm}$ and $W^+W^-W^{\pm}$. The last condition is effective to reduce the SM backgrounds containing top quarks. In the simulation we use the b-tagging efficiency of about 70 %, which is set in the `Delphes` card used in the Snowmass backgrounds.

In order to obtain as large coverage as possible in the $M_2 - \mu$ parameter plane, we define three signal regions: *Loose*, *Medium*, *Tight*. These signal regions are defined in Table 2. The selection cuts are inspired by the kinematical distributions shown in Fig. 6. The *Loose* region, which has the mildest cuts, is designed to constrain the degenerate mass region ($M_2 \gtrsim \mu$), whereas the *Tight* region, which has the hardest cuts, targets the hierarchical mass region ($M_2 \gg \mu$). The *Medium* region is also necessary to extend the coverage in the intermediate mass region.

The visible cross section (the cross section for the events satisfying the event selection requirements) for each signal region is shown in Appendix B. The information for the detailed breakdown of the background contribution and the visible cross section at each step of the selection is also shown. The number of total background events are expected to be 38400, 810 and 12.3 for the *Loose*, *Medium* and *Tight* signal regions, respectively, at 3000 fb^{-1} of integrated luminosity.

5.2 The result

In Fig. 7(a), we show the $2\,\sigma$ exclusion limits in the $\mu - M_2$ parameter plane obtained by the different signal regions. The shaded regions have $S/\sqrt{B} \geq 2$, where S and B are the number of expected signal and background events falling into the signal regions, respectively. For signal we use a constant k-factor of 1.3 across the parameter plane. One can see that the three signal regions are complementary and M_2 can be constrained up to ~ 1.8 TeV for $\mu \lesssim 800$ GeV.

Fig. 7(b) shows the $5\,\sigma$ discovery reach ($S/\sqrt{B} \geq 5$) obtained from the different signal regions. As can be seen, the *Loose* and *Medium* signal regions provide the discovery reach up to about 850 and 1.1 TeV, respectively, for $\mu \lesssim 450$ GeV. On the other hand, the *Tight* signal region does not have sensitivity to $S/\sqrt{B} \geq 5$.

We show in Fig. 8(a) the global $2\,\sigma$ exclusion limits for integrated luminosities of 3000 fb^{-1} (red) and 1000 fb^{-1} (blue). The global exclusion limit is obtained by choosing the signal region that provides the largest $S/\sqrt{B}$ for each mass point. The shaded regions

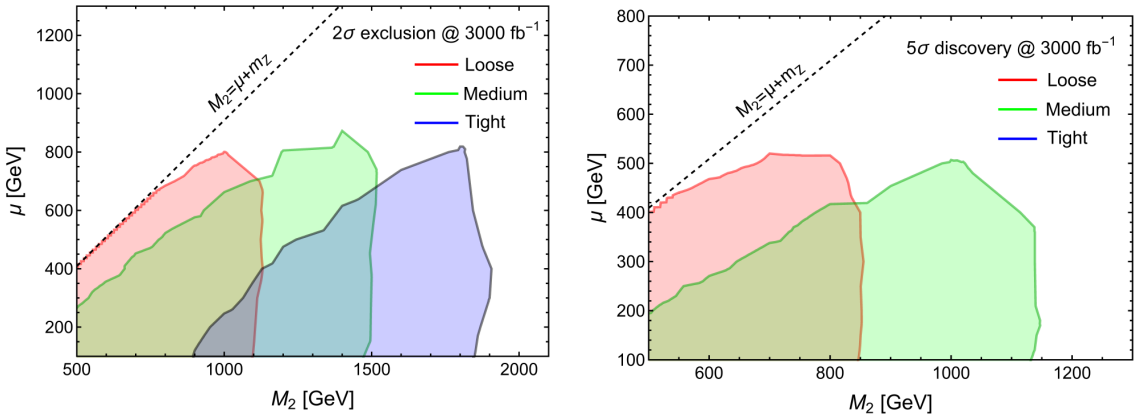

(a) (b)

Figure 7. The exclusion limits (**a**) and the discovery reaches (**b**) obtained from three signal regions. The integrated luminosity of 3000 fb^{-1} is assumed.

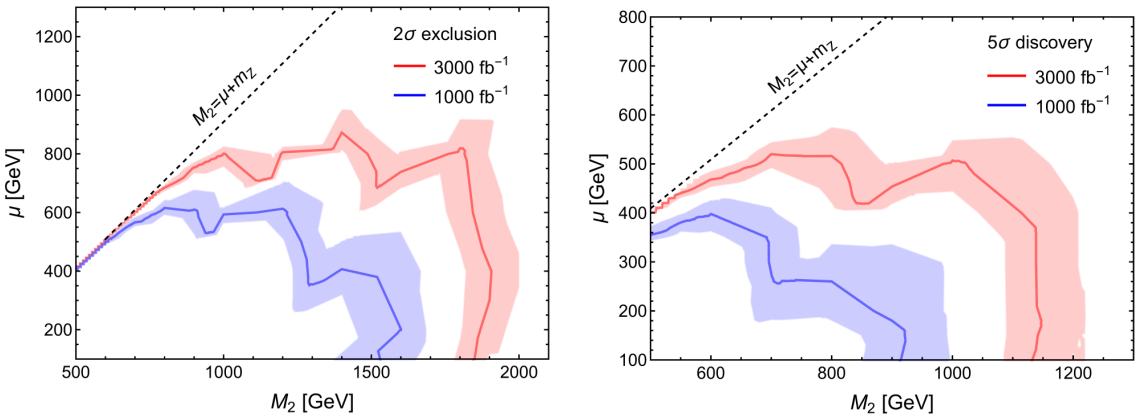

(a) (b)

Figure 8. The global exclusion limits **(a)** and the discovery reaches **(b)** for 3000 fb^{-1} (red) and 1000 fb^{-1} (blue). The shaded region represent the uncertainty when varying the background yield by 30 %.

around the solid curves represent the uncertainty when varying the background yields by ±30 %. One can see that changing the background by 30 % results in a $\sim$ 100 GeV shift in M_2 for the $\mu \ll M_2$ region. M_2 can be constrained up to 1.8 TeV with $\mu \lesssim 800$ GeV for 3000 fb^{-1}, which can be compared with the projected chargino neutralino mass limit of 1.1 TeV for the high luminosity LHC with 3000 fb^{-1} obtained by ATLAS [3]. For 1000 fb^{-1} the limit on M_2 is about 1.5 TeV with $\mu \lesssim 400$ GeV as can be seen in Fig. 8(a).

Fig. 8(b) shows the global 5 σ discovery reach for 3000 fb^{-1} (red) and 1000 fb^{-1} (blue) with the 30 % uncertainty bands for background. One can see that charginos and neutralinos can be discovered up to $M_2 \lesssim 1.1$ TeV with $\mu \lesssim 500$ GeV for 3000 fb^{-1} integrated

luminosity, which can be compared with the projected ATLAS value of 0.8 TeV for the high luminosity LHC [3]. For 1000 fb^{-1}, charginos and neutralinos can be discovered up to 900 GeV with $\mu \lesssim 250$ GeV.

6 Conclusion

In this paper we studied the prospect of chargino and neutralino searches at a 100 TeV pp collider assuming 3000 (1000) fb^{-1} of integrated luminosity. Our particular focus was the case where the Higgsinos form the lightest SUSY states (the lightest charginos and the two lightest neutralinos, which are almost mass degenerate) and W-inos form the second lightest states (the heavier charginos and the third lightest neutralino, which are almost mass degenerate). The other SUSY particles including B-ino are assumed to be decoupled, which is partly motivated by the current LHC results as well as popular scenarios of SUSY breaking and its mediation. We have shown that in this situation the LO production cross sections of 2 TeV W-inos are as large as 100 fb^{-1} and the branching ratio of W-inos follows a simple formula, which can be derived from the Goldstone equivalence theorem.

From a study of kinematic distributions of signal and background we found harsh cuts on lepton p_T ($> 50 - 400$ GeV), $E_T^{\rm miss}$ ($> 150 - 800$ GeV) and m_T ($> 150 - 1100$ GeV) are beneficial to improve the signal and background ratio and designed three complementary signal regions. Using these three signal regions, we found the $5\,\sigma$ discovery reach ($2\,\sigma$ exclusion limit) for the chargino-neutralino mass is 1.1 (1.8) TeV for $\mu \lesssim 500$ (800) GeV, which can be compared with the projected LHC reach (limit) of 0.8 (1.1) TeV obtained by ATLAS [3]. For 1000 fb^{-1} the discovery reach (exclusion limit) for the chargino-neutralino mass is found to be 0.9 (1.5) TeV for $\mu \lesssim 250$ (400) GeV.

Acknowledgments

We would like to thank Lian-Tao Wang, Stefania Gori and Sunghoon Jung for discussions. The work of BSA is supported by the UK STFC via the research grant ST/J002798/1. BSA also acknowledges the hospitality of the Center for the Future for High Energy Physics, Beijing, where this work was first presented. The work of K.S. was supported in part by the London Centre for Terauniverse Studies (LCTS), using funding from the European Research Council via the Advanced Investigator Grant 267352. The work of KB is supported by a Graduate Teaching Assistantship from King's College London.

A The lepton isolation requirement

In hadron colliders, leptons (electrons and muons) may arise from heavy hadron decays. Those "background" leptons are usually found together with other particles around them. The leptons originating from gauge boson decays can therefore be distinguished from the background leptons by investigating activity around the lepton. For this check, `Delphes 3` uses an isolation variable, I, defined as

$$I(\ell) = \frac{\sum_{i \neq \ell}^{\Delta R < R,\ p_T(i) > p_T^{\min}} p_T(i)}{p_T(\ell)}, \tag{A.1}$$

where the numerator sums the p_T of all particles (except for the lepton itself) with $p_T > p_T^{\min}$ lying within a cone of radius R around the lepton. If $I(\ell)$ is smaller than $I_{\min}$, the lepton is said to be isolated, otherwise gets rejected as background. The Snowmass samples were generated using `Delphes 3` with the lepton isolation parameters of $R = 0.3$, $p_T^{\min} = 0.5$ and $I_{min} = 0.1$.

A 100 TeV collider can explore charginos and neutralinos with their mass scale of a few TeV. If the mass hierarchy between W-ino states and Higgsino states are much higher than the gauge bosons mass scale, the W and Z produced from the W-ino decays will be highly boosted. If such a boosted Z decays into a pair of same-flavour opposite-sign (SFOS) leptons, those two leptons can be highly collimated, and one may be rejected by the isolation criteria defined above.

To see the impact of this effect, we show the $\Delta R_{\rm SFOS}$ (the distance between the SFOS pair[3]) distributions in Fig 9. In Fig 9, the background sample consists of the most relevant processes, WZ and ttZ, which we have generated using `MadGraph 5` and `Phythia 6`.[4] For signal, we examine three benchmark points: (M_2, μ)/GeV = (800, 200), (1200, 200) and (1800, 200). The particle level samples are passed to `Delphes 3` with the same detector setup as used in Snowmass but with $R = 0.05$ for the lepton isolation cone radius.

Fig. 9(a) shows the $\Delta R_{\rm SFOS}$ distributions after the preselection cuts. As can be seen, signal events are more concentrated around the small $\Delta R_{\rm SFOS}$ values, while background has rather flat distribution. One can also see that smaller $\Delta R_{\rm SFOS}$ is preferred for model points with larger mass hierarchy.

In Fig. 9(b) we present the same distributions of $\Delta R_{\rm SFOS}$ but with the requirement of $E_T^{\rm miss} > 500$ GeV and $m_T > 200$ GeV on top of the preselection cuts. As can be seen, the distributions are more concentrated for signal and background compared to the distributions with only preselection cuts. This is because the harsh cuts on $E_T^{\rm miss}$ and m_T call for large $\sqrt{\hat{s}}$ for the partonic collision, leading to more boosted Z for both signal and background events. One can see that the significant fraction of events has a SFOS lepton pair lying within $\Delta R_{\rm SFOS} < 0.3$ of each other, and it is expected that the Snowmass lepton

[3] To be explicit, $\Delta R_{\rm SFOS} = \sqrt{(\Delta\phi_{\rm SFOS})^2 + (\Delta\eta_{\rm SFOS})^2}$, where $\Delta\phi_{\rm SFOS}$ and $\Delta\eta_{\rm SFOS}$ are the azimuthal and pseudo-rapidity differences between the SFOS lepton pair.

[4] In the WZ sample, two extra partons are matched with the parton shower radiation with the MLM merging scheme [34].

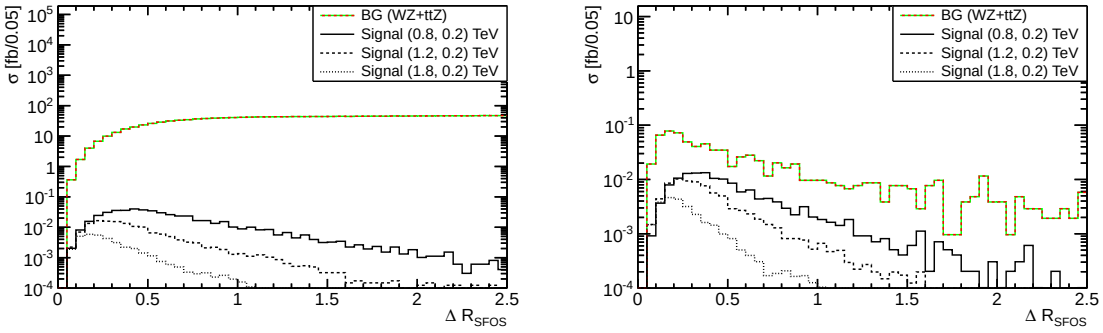

(a) (b)

Figure 9. The distributions of $\Delta R_{\rm SFOS}$, the distance between the SFOS lepton pair, **(a)** after preselection cuts, **(b)** after additional cuts: $E_T^{\rm miss} > 500$ GeV and $m_T > 200$ GeV. For both plots, detector simulation has been done by `Delphes 3` using the same detector setup as the one used in Snowmass samples but with $R = 0.05$.

isolation criteria with $R = 0.3$ would reject some fraction of signal and background events. We therefore believe that employing smaller lepton isolation cone radius will improve the chargino-neutralino mass reach to some extent, although a dedicated study in this direction is beyond the scope of this paper.

B The visible cross sections

In this section we report the visible cross sections (the cross section after cuts) for each step of the selection cuts for different processes. Four sets of samples are considered for the SM background, which are defined in Table 1. We show the results for three benchmark model points for signal: $(M_2, \mu)/\text{GeV} = (800, 200)$, (1200, 200) and (1800, 200). The (visible) cross sections with k-factor = 3 are shown in fb for all tables in this section. Table 3 shows the (visible) cross sections for the cuts employed in the *preselection* stage. Table 4, 5 and 6 show the visible cross sections for the cuts used in *Loose*, *Medium* and *Tight* signal regions, respectively. The last columns in Tables 4, 5 and 6 show $S/\sqrt{B}$ assuming 3000 fb^{-1} of integrated luminosity for the three different benchmark points.

Process	No cut	= 3 lepton	$\lvert m_{\ell\ell}^{\rm SFOS} - m_Z\rvert < 10$	no-b jet
VV	3025348	2487	2338	2176
ttV	220161	792	552	318
tV	2764638	68.9	6.07	4.12
VVV	36276	76.1	56.2	56.2
BG total	6046422	3424	2952	2554
$(M_2, \mu) = (800, 200)$	1.640	0.588	0.565	0.534
$(M_2, \mu) = (1200, 200)$	0.397	0.124	0.119	0.111
$(M_2, \mu) = (1800, 200)$	0.0863	0.0190	0.0179	0.0170

Table 3. The (visible) cross sections (in fb) for the cuts employed in the *preselection*. The column marked "No cut" shows the cross sections for the background processes (defined in Table 1) and the cross section times branching ratio into 3 leptons via WZ for signal benchmark points.

Process	$p_T^\ell > (100, 50, 10)$	$E_T^{\rm miss} > 150$	$m_T > 150$	$S/\sqrt{B}$
VV	647	106	5.1	
ttV	176	41.2	6.6	
tV	0.665	0.391	0.0793	
VVV	23.4	6.0	1.06	
BG total	847	153	12.8	
$(M_2, \mu) = (800, 200)$	0.506	0.465	0.381	5.82
$(M_2, \mu) = (1200, 200)$	0.109	0.103	0.090	1.38
$(M_2, \mu) = (1800, 200)$	0.0168	0.0164	0.0150	0.234

Table 4. The visible cross sections (in fb) used in the *Loose* signal region. The last column shows $S/\sqrt{B}$ assuming the 3000 fb^{-1} luminosity for different benchmark points.

Process	$p_T^\ell > (250, 150, 50)$	$E_T^{\rm miss} > 350$	$m_T > 300$	$S/\sqrt{B}$
VV	33.8	3.13	0.106	
ttV	9.84	0.780	0.119	
tV	0.037	0.0213	0.00132	
VVV	1.87	0.291	0.0442	
BG total	45.6	4.22	0.271	
$(M_2, \mu) = (800, 200)$	0.170	0.107	0.0845	8.89
$(M_2, \mu) = (1200, 200)$	0.0572	0.0463	0.0408	4.30
$(M_2, \mu) = (1800, 200)$	0.0099	0.0088	0.0081	0.845

Table 5. The visible cross sections (in fb) used in the *Medium* signal region. The last column shows $S/\sqrt{B}$ assuming the 3000 fb^{-1} luminosity for different benchmark points.

Process	$p_T^\ell > (400, 200, 75)$	$E_T^{\text{miss}} > 800$	$m_T > 1100$	$S/\sqrt{B}$
VV	5.65	0.123	0.00166	
ttV	1.03	0.0056	0.00092	
tV	0.015	0.0001	0	
VVV	0.350	0.0109	0.00153	
BG total	7.05	0.140	0.00411	
$(M_2, \mu) = (800, 200)$	0.0460	0.0020	0.0012	1.00
$(M_2, \mu) = (1200, 200)$	0.0238	0.0070	0.0052	4.45
$(M_2, \mu) = (1800, 200)$	0.0053	0.0031	0.0026	2.22

Table 6. The visible cross sections (in fb) used in the *Tight* signal region. The last column shows $S/\sqrt{B}$ assuming the 3000 fb^{-1} luminosity for different benchmark points.

References

[1] **ATLAS Collaboration** Collaboration, G. Aad et al., *Search for direct production of charginos, neutralinos and sleptons in final states with two leptons and missing transverse momentum in pp collisions at $\sqrt{s} = 8$ TeV with the ATLAS detector*, JHEP **1405** (2014) 071, [arXiv:1403.5294].

[2] **CMS Collaboration** Collaboration, V. Khachatryan et al., *Searches for electroweak production of charginos, neutralinos, and sleptons decaying to leptons and W, Z, and Higgs bosons in pp collisions at 8 TeV*, arXiv:1405.7570.

[3] **ATLAS** Collaboration, *Search for Supersymmetry at the high luminosity LHC with the ATLAS experiment*, Tech. Rep. ATL-PHYS-PUB-2014-010, CERN, Geneva, 2014.

[4] T. Cohen, T. Golling, M. Hance, A. Henrichs, K. Howe, et al., *SUSY Simplified Models at 14, 33, and 100 TeV Proton Colliders*, JHEP **1404** (2014) 117, [arXiv:1311.6480].

[5] T. Andeen, C. Bernard, K. Black, T. Childres, L. Dell'Asta, et al., *Sensitivity to the Single Production of Vector-Like Quarks at an Upgraded Large Hadron Collider*, arXiv:1309.1888.

[6] L. Apanasevich, S. Upadhyay, N. Varelas, D. Whiteson, and F. Yu, *Sensitivity of potential future pp colliders to quark compositeness*, arXiv:1307.7149.

[7] D. Stolarski, *Reach in All Hadronic Stop Decays: A Snowmass White Paper*, arXiv:1309.1514.

[8] F. Yu, *Di-jet resonances at future hadron colliders: A Snowmass whitepaper*, arXiv:1308.1077.

[9] N. Zhou, D. Berge, L. Wang, D. Whiteson, and T. Tait, *Sensitivity of future collider facilities to WIMP pair production via effective operators and light mediators*, arXiv:1307.5327.

[10] S. Jung and J. D. Wells, *Gaugino physics of split supersymmetry spectrum at the LHC and future proton colliders*, Phys.Rev. **D89** (2014) 075004, [arXiv:1312.1802].

[11] M. Low and L.-T. Wang, *Neutralino Dark Matter at 100 TeV*, arXiv:1404.0682.

[12] M. Cirelli, F. Sala, and M. Taoso, *Wino-like Minimal Dark Matter and future colliders*, arXiv:1407.7058.

[13] L. Randall and R. Sundrum, *Out of this world supersymmetry breaking*, Nucl.Phys. **B557** (1999) 79–118, [hep-th/9810155].

[14] G. F. Giudice, M. A. Luty, H. Murayama, and R. Rattazzi, *Gaugino mass without singlets*, JHEP **9812** (1998) 027, [hep-ph/9810442].

[15] T. Moroi and L. Randall, *Wino cold dark matter from anomaly mediated SUSY breaking*, Nucl.Phys. **B570** (2000) 455–472, [hep-ph/9906527].

[16] B. S. Acharya, K. Bobkov, G. L. Kane, P. Kumar, and J. Shao, *Explaining the Electroweak Scale and Stabilizing Moduli in M Theory*, Phys.Rev. **D76** (2007) 126010, [hep-th/0701034].

[17] B. S. Acharya, K. Bobkov, G. L. Kane, J. Shao, and P. Kumar, *The G(2)-MSSM: An M Theory motivated model of Particle Physics*, Phys.Rev. **D78** (2008) 065038, [arXiv:0801.0478].

[18] B. S. Acharya, G. Kane, and P. Kumar, *Compactified String Theories – Generic Predictions for Particle Physics*, Int.J.Mod.Phys. **A27** (2012) 1230012, [arXiv:1204.2795].

[19] N. Arkani-Hamed and S. Dimopoulos, *Supersymmetric unification without low energy supersymmetry and signatures for fine-tuning at the LHC*, JHEP **0506** (2005) 073, [hep-th/0405159].

[20] G. Giudice and A. Romanino, *Split supersymmetry*, Nucl.Phys. **B699** (2004) 65–89, [hep-ph/0406088].

[21] N. Arkani-Hamed, S. Dimopoulos, G. Giudice, and A. Romanino, *Aspects of split supersymmetry*, Nucl.Phys. **B709** (2005) 3–46, [hep-ph/0409232].

[22] J. Alwall, M. Herquet, F. Maltoni, O. Mattelaer, and T. Stelzer, *MadGraph 5 : Going Beyond*, JHEP **1106** (2011) 128, [arXiv:1106.0522].

[23] S. Jung, *Resolving the existence of Higgsinos in the LHC inverse problem*, JHEP **1406** (2014) 111, [arXiv:1404.2691].

[24] A. Djouadi, M. Muhlleitner, and M. Spira, *Decays of supersymmetric particles: The Program SUSY-HIT (SUspect-SdecaY-Hdecay-InTerface)*, Acta Phys.Polon. **B38** (2007) 635–644, [hep-ph/0609292].

[25] H. Baer, V. Barger, A. Lessa, W. Sreethawong, and X. Tata, *Wh plus missing-E_T signature from gaugino pair production at the LHC*, Phys.Rev. **D85** (2012) 055022, [arXiv:1201.2949].

[26] T. Han, S. Padhi, and S. Su, *Electroweakinos in the Light of the Higgs Boson*, Phys.Rev. **D88** (2013) 115010, [arXiv:1309.5966].

[27] D. Ghosh, M. Guchait, and D. Sengupta, *Higgs Signal in Chargino-Neutralino Production at the LHC*, Eur.Phys.J. **C72** (2012) 2141, [arXiv:1202.4937].

[28] P. Byakti and D. Ghosh, *Magic Messengers in Gauge Mediation and signal for 125 GeV boosted Higgs boson*, Phys.Rev. **D86** (2012) 095027, [arXiv:1204.0415].

[29] A. Papaefstathiou, K. Sakurai, and M. Takeuchi, *Higgs boson to di-tau channel in Chargino-Neutralino searches at the LHC*, arXiv:1404.1077.

[30] J. Anderson, A. Avetisyan, R. Brock, S. Chekanov, T. Cohen, et al., *Snowmass Energy Frontier Simulations*, arXiv:1309.1057.

[31] P. Meade and M. Reece, *BRIDGE: Branching ratio inquiry / decay generated events*, hep-ph/0703031.

[32] T. Sjostrand, S. Mrenna, and P. Z. Skands, *PYTHIA 6.4 Physics and Manual*, JHEP **0605** (2006) 026, [hep-ph/0603175].

[33] **DELPHES 3** Collaboration, J. de Favereau et al., *DELPHES 3, A modular framework for fast simulation of a generic collider experiment*, JHEP **1402** (2014) 057, [arXiv:1307.6346].

[34] M. L. Mangano, M. Moretti, F. Piccinini, and M. Treccani, *Matching matrix elements and shower evolution for top-quark production in hadronic collisions*, JHEP **0701** (2007) 013, [hep-ph/0611129].